Optics and Laser Technology 103 (2018) 1–7

Contents lists available at ScienceDirect

Optics and Laser Technology

journal homepage: www.elsevier.com/locate/optlastec

Full length article

Quantitative analysis of vacuum-ultraviolet radiation from nanosecond laser-zinc interaction

Homaira Parchamy [a,b,*], John Szilagyi [a], Majid Masnavi [a], Martin Richardson [a]

[a] Laser Plasma Laboratory, Townes Laser Institute, The College of Optics and Photonics, University of Central Florida, Orlando, FL 32816, USA
[b] The College of Physics, Florida Polytechnic University, Lakeland, FL 33805, USA

ARTICLE INFO

Article history:
Received 5 July 2017
Received in revised form 4 November 2017
Accepted 4 January 2018

Keywords:
Laser-matter interaction
Laser-produced plasma
Vacuum-ultraviolet spectroscopy
Seya-Namioka monochromator
Radiation-hydrodynamics
Non-local thermodynamic equilibrium population kinetics

ABSTRACT

The paper reports measurements of the vacuum-ultraviolet spectral irradiances of a flat zinc target over a wavelength region of 124–164 nm generated by 10 and 60 ns duration low-intensities, $5 \times 10^9 - 3 \times 10^{10}$ W cm^{-2}, 1.06 μm wavelength laser pulses. Maximum radiation conversion efficiencies of 2.5%/2πsr and 0.8%/2πsr were measured for 60 and 10 ns laser pulses at the intensities of 5×10^9 and 1.4×10^{10} W cm^{-2}, respectively. Atomic structure calculations using a relativistic configuration-interaction, flexible atomic code and a developed non-local thermodynamic equilibrium population kinetics model in comparison to the experimental spectra detected by the Seya-Namioka type monochromator reveal the strong broadband experimental emission originates mainly from $3d^94p$-$3d^94s$, $3d^94d$-$3d^94p$ and $3d^84p$-$3d^84s$, $3d^84d$-$3d^84p$ unresolved-transition arrays of double and triple ionized zinc, respectively. Two-dimensional radiation-hydrodynamics code is used to investigate time-space plasma evolution and spectral radiation of a 10 ns full-width-at-half-maximum Gaussian laser pulse-zinc interaction.

1. Introduction

Technological advances in recent years have increased the demand for the controlled use of short-wavelength light radiation. The vacuum-ultraviolet (VUV, $\lambda \approx 20$—200 nm), extreme-ultraviolet (EUV, $\lambda \approx 10$—20 nm), and soft X-ray (SXR, $\lambda \approx 1$—10 nm) portions of the electromagnetic spectrum have the potential for important applications in the semiconductor industry such as high volume manufacturing lithography and metrology tools [1–11], materials processing of low-*k* dielectrics [12,13], surface modification, and micro-structuring of polymeric materials [14]. In the last few years, laser-produced plasmas (LPPs) have been increasingly considered as pulsed, bright, and broadband light sources from the visible to the X-ray region, due to their intense radiative emission and their small plasma sizes. Most of the industrial effort in LPPs light source experiments is devoted to the microlithography applications in the EUV and X-ray regions. A few studies have so far considered the production of radiation in the long-wavelength VUV region of 100–200 nm [15–25].

In this paper, we report a characterization study of the spectral irradiance of a LPP from a flat bulk zinc (Zn) target under vacuum conditions. To check the feasibility of VUV light-based applications, absolute calibration of the spectral irradiance over a wavelength region of 124–164 nm was carried out. To investigate theoretically the spectral features, we have developed a non-local thermodynamic equilibrium (non-LTE) population kinetics code, the so-called collisional-radiative (CR) model [7,24–27], including excited states in a detail-level accounting approach. The atomic structure of the Zn charge states is calculated using the relativistic configuration-interaction, flexible atomic code (FAC) [28]. The plasma dynamics and time-space-integrated spectral emission are investigated using the CR solver, the equation of radiative transfer in plane-parallel geometry, and two-dimensional (2D) radiation-hydrodynamics code FLASH [29,30].

2. Experimental set-up

In the present study two 1.06 μm lasers were used separately, a Q-switched Nd:YAG solid-state laser producing 10 ns full-width-at-half-maximum (FWHM) pulses at 100 Hz repetition rate and a fiber laser operating at 2000 Hz producing 60 ns FWHM pulses [3,24,25,31]. The output of these laser pulses were focused in vacuum by a 25.4 mm diameter, 60 mm focal length lens onto flat

* Corresponding author at: Laser Plasma Laboratory, Townes Laser Institute, The College of Optics and Photonics, University of Central Florida, Orlando, FL 32816, USA.
E-mail address: HomairaParchamy@creol.ucf.edu (H. Parchamy).

https://doi.org/10.1016/j.optlastec.2018.01.006
0030-3992/

solid Zn targets oriented at ≈45° to the target normal. The schematic of experimental set-up is illustrated in Fig. 1. A light-valve consisting of a half-wave plate and a polarizer was used to change the laser intensity without altering the beam profile. The focused beam of these two lasers generated plasmas in a $\approx 10^{-6}$ Torr vacuum chamber from a rotating disc target with the radius of ≈3 cm and the rotational speed of ≈5 RPM. The surface of Zn target was aligned to the focal plane of the laser, by combination of translation and rotation stages. The target rotational speed was fast enough to provide a fresh sample in every approximately ten laser shots for 60 ns FWHM pulse. Thus, for the 2000 Hz repetition rate, the ablation can be triggered at the lower laser intensity than laser-zinc fresh target interaction. This is due to higher heat accumulation in the target for 2000 Hz, 60 ns pulse than 100 Hz, 10 ns laser beam. Effects related to the use of high repetition rate pulses on the ablation and plasma thresholds [32,33] are now being investigated. In the experiments by the 10 ns FWHM laser, the lens placed close to the target to achieve the low laser intensity region. The laser spot size diameters on the target for the 10 ns and 60 ns pulses are measured to be ≈300 μm and 80 μm, respectively. The spot size is estimated at the point that the laser intensity has dropped to ≈0.135 of its on-axis value. This large laser spot size was necessary to enhance the signal-to-noise ratio of the spectral data recorded using the 10 ns FWHM laser at the low laser intensity region. Before the experiments, we investigated the laser beam distribution on the target by an optical imaging system from the Imaging Source Company with a charge-coupled-device (CCD) camera that utilizes a Sony ICX618ALA CCD sensor with the pixel size of 5.6 m. Our previous studies revealed that the laser intensity of 10 ns pulse is distributed non-uniformly across the cross-section of the laser beam. However, practically, from the calculation point of view, the beam distribution could be estimated by a super-Gaussian profile [25].

The plasma spectral features were characterized using an aberration corrected 234/302 McPherson Seya-Namioka style spectrometer [34,35] with a 1200 groove/mm grating, 200 mm focal length, 0.1 nm achievable spectral resolution (tested at the wavelength of ≈185 nm with the 10μm wide slit), and 4 nm/mm dispersion. The spectrometer receives the plasma emission at an oblique angle of ≈15° with the normal to the target. The optical path of the spectrometer was maintained at the pressure of $\approx 10^{-6}$ Torr. The input 10 μm slit of the spectrometer, 100 cm from the target, has a protective MgF_2 window with a cutoff wavelength at ≈115 nm. The spectrometer was customized with a fiber optic face plate, coupled micro-channel plate (MCP), with a cesium iodide (CsI) photocathode at the output image plane. This photocathode limits the spectral response of the spectrometer to the wavelengths shorter than ≈164 nm. A chilled CCD array (169 μm^2 1024 pixel detector), with a fiber optic face plate was coupled to the MCP's fiber optic face plate.

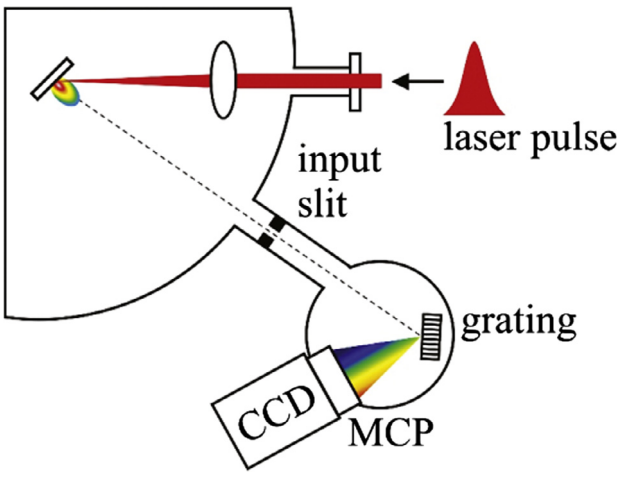

Fig. 1. The schematic of experimental set-up, including a Seya-Namioka type spectrometer featuring a 1200 groove/mm grating, a multi-channel plate (MCP) intensifier, and a chilled charged-couple-device (CCD). Two 1.06 μm lasers were used separately, a Q-switched Nd:YAG solid-state laser producing 10 ns FWHM pulses at 100 Hz repetition rate and a fiber laser operating at 2000 Hz producing 60 ns FWHM pulses to generate plasma from a rotating flat bulk Zn target.

We have investigated the spectral sensitivity of the spectrometer over the wavelength region of 124–164 nm using a standard Deuterium lamp (X2D2, L9841 Hamamatsu). The lamp [36] provides the absolute calibrated irradiance data 100 cm from the lamp over the wavelength region of ≈115 to 300 nm. The detail of the calibration method and the spectral sensitivity curve of spectrometer is discussed in the previous publications [24,25].

3. Computational model

To investigate theoretically the spectral characteristics of Zn plasma radiation, we have constructed a CR balance-rate equation, including excited states in a detail-level accounting approach [24,25]. The CR model includes all of the important atomic processes in a typical LPP light source, such as the autoionization from the doubly excited states and dielectronic recombination, electron impact ionization and three-body recombination, electron impact excitation and deexcitation, photoionization and radiative recombination, photoexcitation, and photodeexcitation. The photoionization, photoexcitation, and photodeexcitation are calculated for a Planckian radiation field. The state-of-the-art configuration-interaction FAC code is used to calculate the necessary atomic data for solving the CR balance equation. The FAC solves the relativistic Dirac equation, using a single central parametric potential to compute the orbitals. Radiative decay, collisional excitation and ionization, autoionization and photoionization cross sections and rates are computed within the distorted wave approximation. The calculated atomic data (e.g., the spectral line positions of the oscillator strengths for different charge states) by the FAC code reveal the low-ionized charge states, especially, the double (Zn III) and triple (Zn IV) should emit strongly over the wavelength region of 100–170 nm. We have therefore included the singly and doubly excited states of Zn I to Zn VI charge states in the CR model (Table 1). The CR model has also included the ground state configurations of Zn VII to Zn IX.

The constructed CR solver depends on three different temperatures for the electron (T_e), ion (T_i), and the radiation field (T_r). Fig. 2a presents the fractional ion populations of an artificial Zn

Table 1
The singly and doubly excited states of zinc included in the CR calculation. Here n and l are, respectively, the principal and orbital quantum numbers. The total levels in the CR are 3342.

State	Transitions
Zn I	$3d^{10}4s^2$, $3d^{10}4s4l$ ($l \leqslant 3$), $3d^{10}4snl$ ($n \leqslant 7$, $l \leqslant 6$), $3d^{10}4p^2$, $3d^9 4s4p^2$
Zn II	$3d^{10}4s$, $3d^{10}4l$ ($l \leqslant 3$), $3d^9 4s^2$, $3d^9 4s4l$ ($l \leqslant 3$), $3d^{10}nl$ ($n \leqslant 7$, $l \leqslant 6$), $3d^9 4p^2$, $3d^9 4d^2$
Zn III	$3d^{10}$, $3d^9 4l$ ($l \leqslant 3$), $3d^9 5l$ ($l \leqslant 3$), $3d^9 6l$ ($l \leqslant 2$), $3d^9 7l$ ($l \leqslant 1$), $3d^8 4s^2$, $3d^8 4p^2$
Zn IV	$3p^6 3d^9$, $3p^5 3d^{10}$, $3d^8 4l$ ($l \leqslant 3$), $3d^8$ $5l$ ($l \leqslant 2$), $3d^8 6l$ ($l \leqslant 1$), $3d^8 7s$, $3d^7 4s^2$, $3d^7 4p^2$
Zn V	$3p^6 3d^8$, $3p^5 3d^9$, $3d^7 4l$ ($l \leqslant 2$), $3d^7 5l$ ($l \leqslant 1$), $3d^6 4s^2$, $3d^6 4p^2$
Zn VI	$3p^6 3d^7$, $3d^6 4s$, $3d^6 4p$
Zn VII	$3p^6 3d^6$
Zn VIII	$3p^6 3d^5$
Zn IX	$3p^6 3d^4$